Conformational Properties and Intrinsic Viscosity of Dendrimers under Excluded-Volume Conditions

Fabio Ganazzoli,*,† Roberto La Ferla,* and Giovanni Terragni

Dipartimento di Chimica, Politecnico di Milano, via L. Mancinelli 7, I-20131 Milano, Italy

Received February 11, 2000; Revised Manuscript Received May 31, 2000

ABSTRACT: The good-solvent expansion of dendrimers is theoretically studied by self-consistent free-energy minimization accounting for all the relevant degrees of freedom. This feature enables a description both of the local conformation and of the overall molecular behavior. Equilibrium and dynamical properties are calculated, in particular the radius of gyration and the viscometric radius (from intrinsic viscosity). The intramolecular swelling is concentrated in the core region, the individual dendra, sub-dendra, etc., being stretched outward with relatively little inter-dendron mixing. Appropriate reduced variables are found for the characteristic radii, which yield a unique master curve for any generation and solvent quality. We also propose an analytical fitting function that permits easy numerical calculation for all cases of interest. The intrinsic viscosity dependence on generation is discussed, including the possible existence of a maximum as experimentally observed in some cases.

Introduction

Dendrimers are a class of hyperbranched molecules that have spurred much interest for their complex, yet regular, architecture.[1,2] Many useful applications have been proposed for these molecules that exploit their topological characteristics. In particular, a wide range of supramolecular complexes have been devised with possible uses as drug controlled-release systems or as gene transfection agents. In addition, since dendrimers have uniform surface chemistry at the terminal groups and minimal mass distribution, dendrimeric covalent conjugates have been synthesized for a number of possible applications, e.g., as catalysts or as intravascular contrast-enhancing agents for magnetic resonance imaging.[1,2] One relevant aspect of these molecules lies in their outer steric congestion. From the topological viewpoint, they may be described as formed by concentric shells defined by the branch points separated by the same number of bonds from the core. Therefore, the number of monomers increases geometrically for each new shell. This feature led to an estimate of the largest number of shells that can actually be added before crowding becomes too large.[3] Describing dendrimer size under excluded-volume conditions is therefore a challenging theoretical problem because of the large number of intramolecular interactions.

In the present paper we report our results about dendrimer expansion using a self-consistent statistical-mechanical approach with minimization of the intramolecular free energy.[4,5] The theory correctly accounts for all the relevant degrees of freedom, in the assumption of a Gaussian distribution for the distances among the beads. In this way, we obtain results both for the overall molecular size and for the intramolecular conformation. Chain dynamics is also investigated so as to get the intrinsic viscosity and the viscometric radius. The equilibrium results for the molecular expansion are taken into account both for the intramolecular elastic forces and for the (preaveraged) hydrodynamic interaction.

* To whom correspondence should be addressed.
† E-mail: Fabio.Ganazzoli@polimi.it.

The plan of the paper is as follows. The next section describes the statistical model for dendrimers with the expressions of the intramolecular free energy and of the quantities of interest. Afterward, we present our equilibrium and dynamic results: we describe both the local conformation and the overall molecular size, as well as the viscometric properties. We also find master curves summarizing our results in terms of appropriate universal variables and propose an analytical fit to the calculated radii through Hill functions. Afterward, we compare the predicted generation dependence of the radii with theoretical scaling laws and with experimental and simulation data. In the final section we briefly summarize the main issues and give an outlook of future work. A fuller account of dendrimer dynamics will be reported in a separate paper.[6]

Theoretical Method

We consider dendrimers formed by f trees of order m (the dendra) connected to a central core and comprising P bonds between neighboring branch points. The molecular topology can be viewed as consisting of a sequence of concentric layers. The outmost layer defines the dendrimer generation g, which is numbered from 0 (no branch point beyond the central core) onward. The total number of beads n is then given by

$$n = 1 + fP\,\frac{m^{g+1} - 1}{m - 1} \tag{1}$$

In the following, we report results for dendrimers with P equal to 1 or 2 having a ternary core ($f = 3$) and binary dendra ($m = 2$), so that each branch point is trifunctional. Therefore, we simply denote our dendrimers as DP-Gg; conversely, linear chains comprising n beads will be indicated as Ln. Scheme 1 shows examples of the dendrimers considered by us, with the numbering pattern of the beads. Freely jointed "bond" vectors of unit length connect adjacent beads with an outward direction (see again Scheme 1); in dynamics, we adopt the bead-and-spring model, a spring of unit mean-square length simply replacing a segment.

10.1021/ma000258+ CCC: $19.00
Published on Web 07/19/2000

Scheme 1

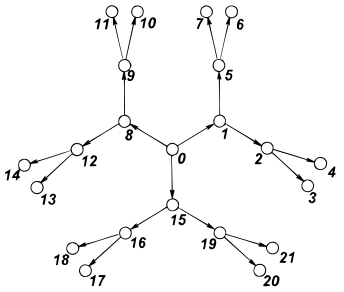

D1–G2

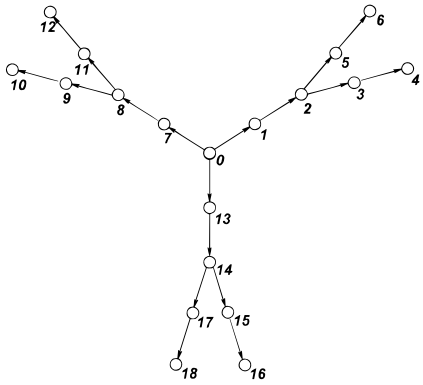

D2–G1

We choose the average scalar products among the $n - 1$ bond vectors describing the dendrimer conformation as the variables to be optimized.[4] The scalar products are conveniently collected in matrix **M**, with elements

$$M_{ij} = \langle \mathbf{l}_i \cdot \mathbf{l}_j \rangle \tag{2}$$

From these quantities we get all the quadratic lengths of interest. In particular, the mean-square distance between the generic beads i and j, $\langle r_{ij}^2 \rangle$, is given by[7]

$$\langle r_{ij}^{\,2} \rangle = \sum_{u=1}^{D_{ij}} \sum_{v=1}^{D_{ij}} U(u,v) \langle \mathbf{l}_{b(u)} \cdot \mathbf{l}_{b(v)} \rangle \tag{3}$$

where the bond index $b(u)$ identifies the uth step of the shortest path going from bead i to bead j and D_{ij} is the topological distance between the two beads. Also, $U(u,v) = \pm 1$ is the sign function that takes into account the sense of the path in view of the definition of the vector directions.

The average scalar products also yield the intramolecular free energy A, which must be optimized self-consistently in order to get the equilibrium conformation.[5] We take the phantom molecule devoid of any intramolecular interaction as our reference state; it shall be indicated in the following with a "ph" subscript. The excess free energy in $k_B T$ units is expressed as[4,5]

$$A = A_{el} + A_2 \tag{4}$$

Here, the elastic part due to the configurational entropy is[4,8]

$$A_{el} = \frac{3}{2}[\mathrm{Tr}\ \mathbf{M} - (n-1) - \ln \mathrm{Det}\ \mathbf{M}] = -\frac{3}{2} \ln \mathrm{Det}\ \mathbf{M} \tag{5}$$

in view of the equality $\mathrm{Tr}\ \mathbf{M} = \sum_{i=1}^{n-1} \langle |\mathbf{l}_i|^2 \rangle = n - 1$, which always holds for constant bond lengths.[4] The two-body interaction free energy is taken as proportional to the probability density of contact among all the bead pairs in the Gaussian approximation[5]

$$A_2 = \tau B \sum\sum_{i<j} \langle r_{ij}^{\,2} \rangle^{-3/2} \tag{6}$$

Here, τB is proportional to the binary cluster integral of the beads and is written as the product of the adimensional covolume per bead B and of the reduced temperature $\tau = (T - \Theta)/T$. Θ is therefore the temperature that makes the binary cluster integral equal to zero. We consider $T > \Theta$, so that A_2 indeed yields a repulsive potential. An extensive discussion on the derivation of the above free energy equations and of the assumptions and approximations they involve can be found in refs 5, 8, and 9.

The self-consistent minimization of A with respect to the scalar products is carried out by exploiting as far as possible the molecular symmetry, as described in the Appendix. From the equilibrium values, we get the mean-square radius of gyration

$$\langle R_S^{\,2} \rangle = \frac{1}{n^2} \sum\sum_{i<j} \langle r_{ij}^{\,2} \rangle \tag{7}$$

and the mean-square distance of the generic bead i from the center of mass

$$\langle R_i^{\,2} \rangle = \langle (\mathbf{r}_i - \bar{\mathbf{r}})^2 \rangle \tag{8}$$

where $\mathbf{r}_i$ is the vector position of the bead and $\bar{\mathbf{r}} = (1/n) \sum_{i=0}^{n-1} \mathbf{r}_i$ is the vector position of the center of mass. Using the cosines theorem and eq 7, we may also write

$$\langle R_i^{\,2} \rangle = \frac{1}{n} \sum_{j=0}^{n-1} \langle r_{ij}^{\,2} \rangle - \langle R_S^{\,2} \rangle \tag{9}$$

The dynamics is studied following Zimm's approach with preaveraged hydrodynamic interaction.[7,10,11] The force constant matrix **A** is obtained by inverting matrix **M**:

$$\mathbf{A} = \mathbf{G} \cdot \mathbf{M}^{-1} \cdot \mathbf{G}^{\mathbf{T}} \tag{10}$$

Here, **G** is the incidence matrix which depends only on the molecular topology.[7] The hydrodynamic interaction is embodied in matrix **H** with elements

$$H_{ij} = \delta_{ij} + (1 - \delta_{ij}) \zeta_r \left\langle \frac{l}{r_{ij}} \right\rangle \tag{11}$$

In the Gaussian approximation the average reciprocal distances are given by

$$\langle r_{ij}^{\,-1} \rangle = \left(\frac{6}{\pi \langle r_{ij}^{\,2} \rangle} \right)^{1/2} \tag{11'}$$

while

$$\zeta_r = \frac{\zeta}{6\pi\eta_0 l} \tag{11''}$$

is the reduced friction coefficient (here set equal to 0.25), ζ being the bead friction coefficient and η_0 the solvent viscosity. The eigenvalues of $\mathbf{H} \cdot \mathbf{A}$ yield the relaxation rates of the normal modes of motion, τ_p^{-1}, $p = 1, 2, \ldots, n - 1$, and a zero eigenvalue related to the diffusion of

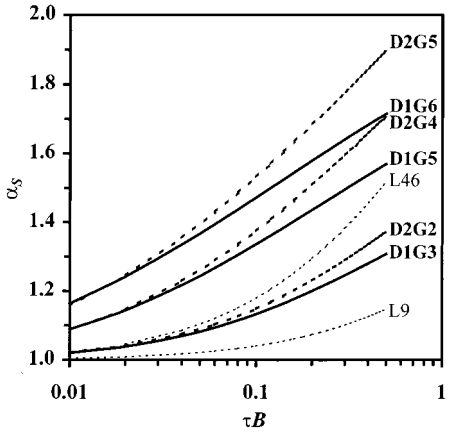

Figure 1. Expansion factor of the radius of gyration α_S plotted as a function of τB for selected generations of D1 and D2 dendrimers (solid and dashed lines, respectively) and for some linear chains (thin dashed lines). The curves are interrupted at $\tau B = 0.5$ for clarity.

the center of mass. From the latter, we get the hydrodynamic radius[11]

$$R_h = n\zeta_r l\left[1 + \frac{\zeta_r}{n}\sum_{i=0}^{n-1}\sum_{\substack{j=0\\ j\neq i}}^{n-1}\left\langle\frac{l}{r_{ij}}\right\rangle\right]^{-1} \qquad (12)$$

Finally, the intrinsic viscosity is given by the sum of the relaxation times τ_p:[10,11]

$$[\eta] = \frac{RT}{2M\eta_0}\sum_{p=1}^{n-1}\tau_p \qquad (13)$$

where M is the molar mass. We also introduce the viscometric radius R_η through Einstein's expression for a hard sphere:[12]

$$[\eta] = \frac{10}{3}\pi\frac{N_{Av}}{M}R_\eta^3 \qquad (14)$$

A more thorough discussion of the relaxation times and of the intramolecular dynamics under excluded-volume conditions is deferred to a future paper.[6]

Discussion

General Results: Molecular Size and the Local Expansion. General results for the dendrimer sizes are reported in Figure 1 together with results from some linear chains for a comparison. We show the expansion factor of the radius of gyration $\alpha_S = R_S/R_{S_{ph}}$ (where $R_S \equiv \langle R_S^2\rangle^{1/2}$) plotted as a function of τB, which gives the strength of the two-body interactions (see eq 6) and therefore embodies the solvent quality. $R_{S_{ph}}$, the radius of gyration of the phantom molecule, is reported in Table 1 together with its analytical expression.[7] The crossover to the finite expansion eventually achieved by dendrimers can be detected through use of the logarithmic abscissa in Figure 1. This feature is particularly evident in dendrimers D1-G5 and D1-G6, while it requires larger τB values in the other cases (not shown for clarity). Thus, due to the compact topology of these molecules and to the steric crowding of the outer beads, α_S shows an early crossover to a finite, asymptotic value.

Table 1. Radius of Gyration[a] $R_{S_{ph}}$, Hydrodynamic Radius $R_{h_{ph}}$, and Viscometric Radius $R_{\eta_{ph}}$ of the Phantom D1 and D2 Dendrimers as a Function of Generation g

	D1			D2		
g	$R_{S_{ph}}$	$R_{h_{ph}}$	$R_{\eta_{ph}}$	$R_{S_{ph}}$	$R_{h_{ph}}$	$R_{\eta_{ph}}$
0	0.7500	0.5306	0.6123	0.9897	0.6997	0.8438
1	1.0817	0.8061	0.9940	1.4471	1.0880	1.3869
2	1.3704	1.0951	1.4317	1.8529	1.4872	2.0034
3	1.6356	1.3920	1.9599	2.2291	1.8974	2.7440
4	1.8819	1.6853	2.6085	2.5805	2.3059	3.6518
5	2.1111	1.9651	3.4109	2.9088	2.6993	4.7740
6	2.3249	2.2253	4.4073			

[a] $R_{S_{ph}} \equiv [\langle R_S^2\rangle_{ph}]^{1/2}$ was derived in ref 7 and is given by $\langle R_S^2\rangle_{ph} = W(f,m,g,P)/n^2$; $W(f,m,g,P) = P^3W(f,m,g,1) - \{[fP(P-1)(c-1)]/6(m-1)^2\}[3fP(c-1) + 2(P+1)(m-1)]$; $W(f,m,g,1) = [f/(m-1)^3][c^2(fhm - fh - f - m) + c(2f + fh - fhm - h + hm^2) - f + m]$, where $c = m^h$ and $h = g + 1$.

D2 dendrimers are more expanded than D1 dendrimers both at the same generation g and at the same beads number (roughly). This feature can be seen in Figure 1 by comparison of D2-G5 with D1-G5 (same generation) and of D2-Gg with D1-G(g+1), $g = 2, 4, 5$ (same number of beads, approximately). Only in the perturbative regime of small τB do the expansion factors α_S of dendrimers D1-Gg and D2-G(g+1) merge into the same curve. Moreover, at any τB dendrimers show a larger expansion than the linear chains having the same topological end-to-end separation (in dendrimers we refer to the farthest ends) because of their steric congestion, as seen by comparing D1-G3 with L9 in Figure 1. On the other hand, dendrimers undergo a much smaller expansion than the linear chain with the same number of beads (compare for instance D1-G3 with L46). This is obviously due to the topological constraints, which are strongest in D1 dendrimers.

We can better understand the dendrimer expansion pattern by analysis of their local conformation. It turns out that the molecular expansion is mostly concentrated within each dendron in the core region, just as it happens in regular star polymers.[9,13] This is shown in Figure 2 by the scalar products $\langle \mathbf{l}_i \cdot \mathbf{l}_j \rangle$ between neighboring bonds sequentially connected (i.e., not sprouting from the same branch point). The variable on the abscissa identifies the bead shared by vectors $\mathbf{l}_i$ and $\mathbf{l}_j$, whose label is given by P•s in Scheme 1: the s values ($s = 1, 2, \ldots, g$) define the shells comprising the branch points at the same topological distance from the core. Thus, half-integer abscissas for D2 dendrimers (Figure 2b) correspond to bond pairs comprised within consecutive shells where the common bead is *not* a branch point. The value $s = 0$ indicates the core bead, and the corresponding quantity in Figure 2 is $|\langle \mathbf{l}_i \cdot \mathbf{l}_j \rangle|$ in view of the bond-vector definition (see again Scheme 1).

Figure 2 shows that the scalar products between consecutive bonds in a head-to-tail connection are always positive, so that these vectors form a wider bond angle than in the phantom molecule. Moreover, at any shell these bond angles become larger with increasing dendrimer generation due the greater crowding of the outer beads. In D1 dendrimers the angle between consecutive bonds increases above the core value to a maximum at the first shell (or at the second shell in the most congested dendrimer D1-G6), and afterward it decreases rapidly moving to the outer shells. Thus, dendron expansion is mostly concentrated around the first (and possibly the second) shell, so as to better relieve the steric congestion of the outer beads.

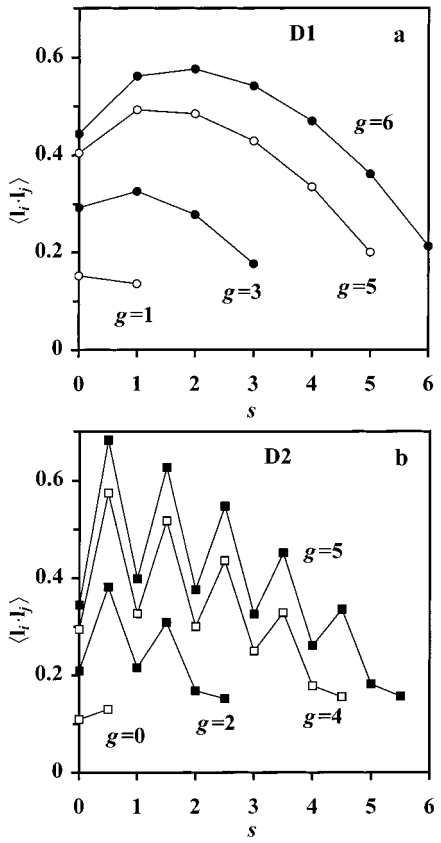

Figure 2. Scalar product $\langle \mathbf{l}_i \cdot \mathbf{l}_j \rangle$ formed by neighboring, sequentially connected bonds vs the shell index s of their common bead at selected generations of D1 and D2 dendrimers. Empty and filled symbols are used for clarity. The results are for $\tau B = 0.5$.

On the other hand, the seesaw pattern of D2 dendrimers in Figure 2b indicates that the adjacent bonds comprised within consecutive shells (half-integer values of the abscissa) form much wider bond angles than those comprising a branch point as the common bead (integer values of the abscissa). Interestingly, the scalar products between geminal bonds sprouting from the same branch point (not reported) indicate large bond angles only at the central core and then show a much smaller opening than the angles between consecutive bond vectors comprising the same common bead. Furthermore, these geminal scalar products quickly tend to the phantom-molecule values in the most congested dendrimers and may also become slightly compressed.

To understand the above pattern, let us note that the repulsion among *different* dendra, or among different sub-dendra, sub-sub-dendra, and so on, must be minimized simultaneously with the optimization of the *intra*-dendron interactions. This is achieved through a large opening of the angle formed by consecutive bonds and a small opening, if any, of the angle between geminal bonds. This expansion pattern brings apart most efficiently consecutive branch points and thus relieves the repulsions both within the dendron (or the sub-dendron, etc.) and among the dendra (or the sub-dendra, etc.). Interestingly, in D2 dendrimers this result implies that bond correlation may also decrease nonmonotonically with topological separation, with shallow local minima when both bonds sprout from branch points of different shells within the same sub-dendron.

As a result, the beads are pushed far from the center of mass, as shown in Figure 3 by the mean-square

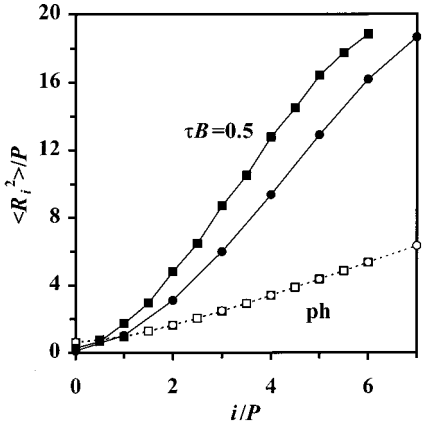

Figure 3. Normalized mean-square distances of the beads from the center of mass as a function of topological distance from the core (see text). Circles are for dendrimer D1-G6 and squares for D2-G5. The normalizing factor P, i.e., the number of bonds between neighboring branch points, also yields the corresponding mean-square distance for the phantom molecule in bond length units.

distances of the beads from the center of mass in the largest-generation dendrimers. Only the core bead gets closer to the center of mass: this result is not unexpected, being consistent with a more spherical shape of branched chains in a good solvent compared to the phantom state.[14,15]

As said before, the dendrimer expansion pattern is qualitatively similar, though obviously more pronounced, to that found in star polymers:[9,13] here, the individual arms undergo a large expansion, mostly in the core neighborhood, while the arms directions are basically uncorrelated so as to minimize their mutual interferences. Our discussion about dendrimer expansion may be summarized by saying that in good solvents the dendra (and the sub-dendra, etc.) tend to be somewhat more segregated than in phantom molecules. Interestingly, this result is consistent with Monte Carlo simulations by Mansfield.[16]

The expansion factors of other dendrimer sizes are shown in Figure 4, where we report the expansion factors of the hydrodynamic radius $\alpha_h = R_h/R_{h_{ph}}$ and of the viscometric radius $\alpha_\eta = R_\eta/R_{\eta_{ph}} = ([\eta]/[\eta]_{ph})^{1/3}$ plotted as a function of τB, the parameter of the two-body interactions, in comparison with the same linear chains as in Figure 1. Unlike the radius of gyration, these radii also depend on the hydrodynamic interaction, which is accounted for within the preaveraging approximation. This approximation becomes inaccurate in stars with more than about nine arms,[17,18] due to the large bead concentration near the core. Therefore, since this effect may be equally severe in dendrimers, we present our results with a word of caution.

In agreement with previous results from linear chains and regular star polymers,[19] we always find the inequality $\alpha_S > \alpha_h > \alpha_\eta$ to hold. Incidentally, α_S^2 is even larger than α_η^3 both in dendrimers and in linear chains, at least within the present τB range. This result, though apparently surprising, is in agreement with previous analytical results on star polymers,[19] as well as with perturbative results on linear chains[12,20] (within the preaveraging approximation), although breaking down in the asymptotic limit. Thus, the radius of gyration undergoes the largest expansion and the viscometric radius the smallest one. It must be noted that the molecular expansion is strongly nonaffine, being

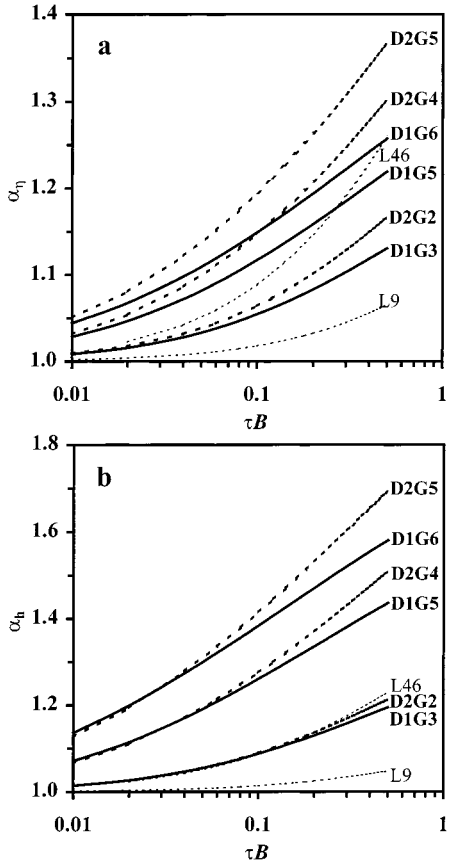

Figure 4. Same as in Figure 1 for the expansion factors of the viscometric radius α_η (a) and of the hydrodynamic radius α_h (b).

largest for topologically distant beads and smallest for nearby beads (or nil for connected beads). Equation 7 shows that the former distances dictate the expansion of the radius of gyration, whereas the latter ones have a larger weight in the hydrodynamic radius (see eq 12). As to the viscometric radius, its expansion is affected by the different decrease rates both of the hydrodynamic interaction and of the force constants, so that an explanation for its small value is not trivial.

The Search for a Master Curve and the Universal Variables. To describe the data by simple and possibly universal functions, let us point out that analytical equations reproducing the calculated α_S strongly depend on the asymptotic maximum value $\alpha_{S_{max}} = R_{S_{max}}/R_{S_{ph}}$ dictated by the connectivity constraints. In fact, Figure 1 suggests that large expansion factors are needed in order to accurately describe the whole behavior of α_S.

After trying various functional forms, we eventually chose a Hill function to describe the behavior of $\alpha_S - 1$, including also its finite asymptote. The general form of this function, first introduced to describe saturation phenomena,[21] can be written as

$$\alpha_S \cong 1 + A_H \frac{x^H}{x_{1/2}{}^H + x^H} \qquad (15)$$

where A_H, $x_{1/2}$, and H are the fit parameters. In this equation, x is an appropriate reduced variable, while $1 + A_H$ yields the asymptotic value $\alpha_{S_{max}}$ and $x_{1/2}$ is the abscissa value yielding one-half of the maximum increase above unity. It is possible to show that the Hill function is equivalent to a logistic function in the logarithmic abscissa scale. In fact, a sigmoidal shape can be detected in the semilogarithmic plots of α_S vs τB in Figure 1.

Table 2. Best-Fit Parameters for the Description of the Excluded-Volume Expansion of R_S (See Eq 16); $R_{S_{max}}(g=0)$ Values Are Imposed in Constrained Fits

		D1	D2
max expansion $R_{S_{max}}$ (eq 18)	$R_{S_{max}}(g=0)$	$(3/4)^{1/2}$	$(15/7)^{1/2}$
	$k_{S_{max}}$	0.652	1.255
	γ	0.943	0.856
	rms error	±0.56%	±0.81%
universal scaling variable ($\beta_S \tau B n^\varphi$)	φ	0.923	
	β_S	(1)	0.602
Hill master curve[a] (eq 16)	$x_{1/2}$	20.33	
	H	0.750	
	rms error on α_S	±0.36%	

[a] Values obtained by minimization of the relative square deviations of α_S (336 data, $g \geq 1$), with simultaneous optimization of $R_{S_{max}}(g,P)$ values to be fitted by eq 17.

Initially, we carried out separate fits for the different structures. It turned out that the τB values for half-expansion scaled with a good approximation as a suitable power of the number of beads. Therefore, it is possible to build a single master curve with all the α_S data plotted against the universal variable $x = \tau B n^\varphi$, where the parameters φ, $x_{1/2}$, and H are independent from generation, while A_H in eq 15 is given by $\alpha_{S_{max}} - 1$ for the corresponding generation. In terms of the Hill function, the master curve for each dendrimer family can be expressed as

$$\frac{\alpha_S - 1}{\alpha_{S_{max}} - 1} = \frac{R_S - R_{S_{ph}}}{R_{S_{max}} - R_{S_{ph}}} \cong \frac{x^H}{x_{1/2}{}^H + x^H} \qquad (16)$$

Recently, on the basis of Monte Carlo simulations, Chen and Cui[22] suggested that R_S scales with $(n-1)^{1-\nu'}(g+1)^{2\nu'-1}$. However, any variable scaling with some power of n can also be scaled with an additional power-law dependence on g, at least in the restricted range of generations which are possible for regular dendrimers. Anyway, no fit based on the scaling variables $n^\varphi(g+1)^\mu$ or $(n-1)^\varphi(g+1)^\mu$ did yield a significant improvement. In addition, we point out that the $R_{S_{ph}}$ values computed by Chen and Cui[22] are approximate, since they assumed the center of mass to coincide with the core, which obviously leads to incorrect values for α_S. The correct expression for $R_{S_{ph}}$ obtained by one us[7] was independently derived by Boris and Rubinstein[23] for the special case of D1 dendrimers. Note that our universal variables for dendrimer expansion account both for a change in the interaction strength (i.e., in τB) and for a change in the number of beads n or equivalently in the generation g. We also point out that as a rule well-defined scaling laws can be expected only in the high-generation limit, which is problematic in regular dendrimers.

Apart from less successful attempts with other functional forms, we tried also a number of possible fits of the data through application of different constraints and data pooling. When all results with D1 and D2 dendrimers are considered into a unique master curve (neglecting only the cases with $g = 0$), the best fit is obtained for eq 16 with $x_{1/2}$ and H reported in Table 2. The "universal" variable x is $\beta_S \tau B n^\varphi$, where β_S is

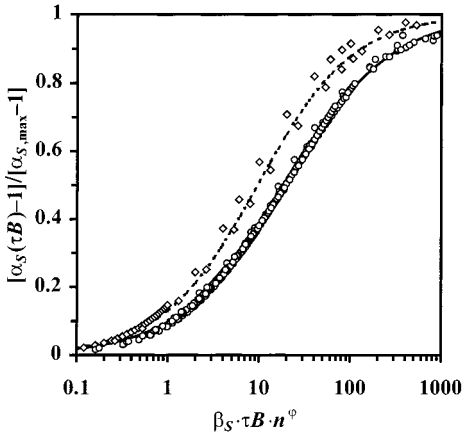

Figure 5. Best fit of a Hill saturation curve (solid line) to calculated results (circles) for α_S as a function of the universal variable (see eq 16 and Table 2 for parameter values). Star structures ($g = 0$) are shown with diamonds and are described by a different saturation curve (dotted curve) plotted as a function of $\tau Bn^{0.5}$ (see text).

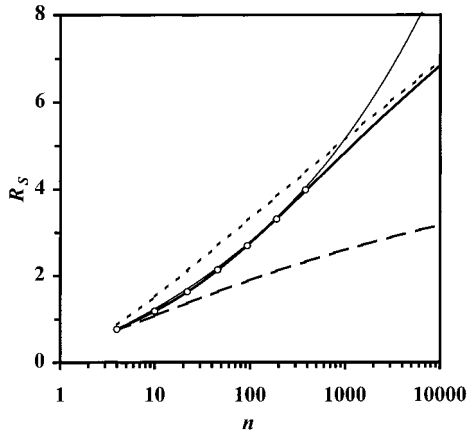

Figure 6. Radius of gyration R_S of D1 dendrimers at $\tau B = 0.5$ (circles) plotted as a function of the number of beads n. The master curve obtained with eqs 16 and 17 is shown with the thick curve, while the thin curve shows the scaling result of Chen and Cui[22] ($R_S \propto (n-1)^{1-\nu'}(g+1)^{2\nu'-1}$, $\nu' = 0.589$). The dotted and dashed lines respectively indicate $R_{S_{max}}$ and $R_{S_{ph}}$ (see text). All values are in bond length units.

different from 1 only for D2 dendrimers (see Table 2). No P dependence can be inferred from two classes of structures only. However, we stress that our universal master equation describes with very good accuracy the expansion data of two different families of dendrimers, both from very low to congested generation and from null to asymptotic (maximum) expansion. Such features are not found in other treatments of experimental or simulations data expressing analytical relationships through scaling laws. The master curve of eq 16 is shown in Figure 5 in comparison with the numerical results, and the fitted parameters are in Table 2. Note that for linear and regular star polymers the universal variable[24,25] is $\tau Bn^{(4-d)/2}$, where d is the space dimensionality. Therefore, compared with an exponent $\varphi = 0.5$ for $d = 3$ and of $\varphi = 1$ for $d = 2$, our value $\varphi = 0.923$ (see Table 2) is consistent with the fact that a large fraction of beads lies near the molecular surface.

The data for $g = 0$ were not considered in the above fit, since these molecules have a star topology. The universal variable for this case is $x = \tau Bn^{0.5}$. Therefore, Figure 5 also reports a Hill function fit ($x_{1/2} = 9.533$, $H = 0.840$) using this variable for such molecules: deviations from a universal behavior are due to the extremely small size of these stars.

With the simultaneous fit of the saturation Hill function to all the data, reliable extrapolations to the asymptotic values are obtained, which can be accurately described by simple equations. A notable result is that the asymptotic radius of gyration $R_{S_{max}}$ depends on the generation g according to a simple power law

$$R_{S_{max}} = (1 + A_H)R_{S_{ph}} \cong R_{S_{max}}(g{=}0) + k_{S_{max}}g^{\gamma} \qquad (17)$$

where $R_{S_{max}}(g{=}0)$ can be calculated as $(3/4)^{1/2}$ for D1 and as $(15/7)^{1/2}$ for D2 dendrimers. This result is not unexpected; in fact, if only repulsion from the center were present, then the maximum possible distance of the beads from the core would depend linearly on their shell level. In this case, with D1 dendrimers one would obtain $R_{S_{max}}$ equal to $(3/4)^{1/2}$, $(27/10)^{1/2}$, $(135/22)^{1/2}$, and so on, tending to $(2 + g^2)^{1/2}$. The actual $R_{S_{max}}$ must also account for the repulsion among the beads belonging to the same dendron and to the same shell, which decreases the radius of gyration. However, the extrapolated $R_{S_{max}}$ still shows an almost linear dependence on g. The best-fit parameters of eq 17 are also reported in Table 2.

The present results provide an analytical description of dendrimer expansion that is by far more precise than any scaling law. When eqs 16 and 17 are written as a function of n only ($g = \log_2[(n + 2)/6]$ for D1, $g = \log_2[(n + 5)/12]$ for D2 dendrimers; see eq 1), the radius of gyration would show an apparent scaling exponent $\nu_{app} = \partial \log R_S/\partial \log n$, which depends both on the interaction parameter τB and on the dendrimer generation g, hence on n. For instance, with $\tau B = 0.5$ the apparent scaling law changes in D1 dendrimers from $n^{0.43}$ for $g = 1$ to $n^{0.23}$ for $g = 6$. The latter exponent agrees well with the relationship $R_S \propto n^{0.22}P^{0.5}$ obtained at large n (large g) by Lescanec and Muthukumar[26] through computer simulations using a self-avoiding kinetic growth algorithm. It is also interesting to note that the scaling law obtained by Chen and Cui[22] as $(n-1)^{1-\nu'}(g+1)^{2\nu'-1}$ with $\nu' = 0.589$ agrees with our results: their apparent scaling law slightly changes from $n^{0.43}$ to $n^{0.41}$ in D1 ($g = 1{-}6$) and from $n^{0.42}$ to $n^{0.41}$ in D2 dendrimers ($g = 1{-}5$). In Figure 6 our results for D1 dendrimers at $\tau B = 0.5$ are shown with circles together with the master eq 16 and to the scaling curve of Chen and Cui.[22] It may be observed that the latter curve coincides with our calculated values up to $g = 6$. At higher generations, however, the scaling law increases without bound, whereas the extrapolation based on our master curve appears to yield more realistic values in the high-g (high-n) limit.

A master curve for the viscometric radius R_η was also obtained by a procedure similar to that employed for R_S. (Due to the similar behavior of R_S and R_h, no master curve is reported for the latter radius for brevity.) In this case, eq 16 becomes

$$\frac{\alpha_\eta - 1}{\alpha_{\eta_{max}} - 1} = \frac{R_\eta - R_{\eta_{ph}}}{R_{\eta_{max}} - R_{\eta_{ph}}} \cong \frac{x^H}{x_{1/2}{}^H + x^H} \qquad (18)$$

with $x = \beta_\eta \tau Bn^{\xi}$ and parameter values reported in Table 3 ($\beta_\eta \neq 1$ for D2 dendrimers). The resulting curve is shown in Figure 7 in comparison with the numerical results. As done before, the corresponding results for

Table 3. Best-Fit Parameters for the Description of the Excluded-Volume Expansion of R_η (See Eq 18); Best-Fit Parameters for Eqs 20 and 21 Are Obtained from Data with $g \geq 1$

		D1	D2
$R_{\eta_{ph}}$ (eq 20)	$k_{\eta_{ph}}$	1.037	1.019
	δ	0.863	0.845
	rms error	±0.08%	±0.11%
max expansion $R_{\eta_{max}}$ (eq 21)	$k_{\eta_{max}}$	1.243	1.369
	ϵ	0.941	0.923
	rms error	±1.82%	±1.56%
universal scaling variable ($\beta_\eta \tau B n^\xi$)	ξ	0.735	
	$\beta\eta$	(1)	0.790
Hill master curve[a] (eq 18)	$x_{1/2}$	11.19	
	H	0.787	
	rms error on α_S	±0.14%	

[a] Values obtained by minimization of the relative absolute square deviations of α_η (336 data, $g \geq 1$), with simultaneous optimization of $R_{\eta_{max}}(g,P)$ values fitted by eq 21.

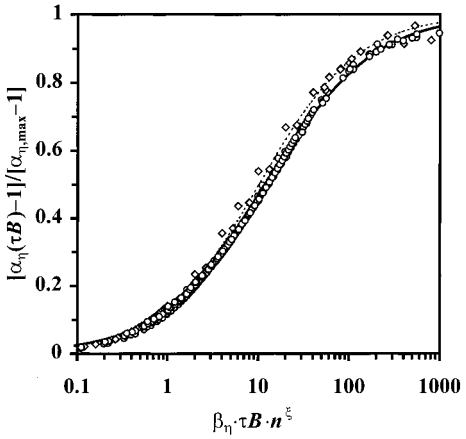

Figure 7. Best fit of a Hill saturation curve (solid line) to calculated results (circles) for α_η as a function of the universal variable (see eq 18 and Table 3 for parameter values). Star structures ($g = 0$) are shown with diamonds and are described by a different saturation curve (dotted curve) plotted as a function of $\tau B n^{0.5}$ (see text).

zero-generation dendrimers were separately fitted using the scaling variable $x = \tau B n^{0.5}$ with a slightly different saturation curve.

Explicit expressions of $R_{\eta_{ph}}$ and of $R_{\eta_{max}}$ are required for an analytical description of the g dependence of the intrinsic viscosity under different excluded-volume conditions through eq 18. However, an analytical formula for $R_{\eta_{ph}}$ in partial draining conditions does not exist, unlike for $R_{S_{ph}}$. Furthermore, we need a reliable extrapolation to the maximum radius, as in the case of R_S. A number of different fits of the numerical data were tried, and the most accurate ones for the calculated $R_{\eta_{ph}}$ and the extrapolated $R_{\eta_{max}}$ were obtained as functions of the free-draining viscometric radius $R^{f.d.}_{\eta_{ph}}$ of the phantom molecule, given by[5,12]

$$R^{f.d.}_{\eta_{ph}} = \left(\frac{3\zeta_r}{10} n l R^2_{S_{ph}}\right)^{1/3} \quad (19)$$

$R_{S_{ph}}$ being reported in Table 1. Equation 19 yields values that are somewhat halfway between $R_{\eta_{ph}}$ and $R_{\eta_{max}}$. The best two-parameters fitting functions were found to be

$$R_{\eta_{ph}} = k_{\eta_{ph}} (R^{f.d.}_{\eta_{ph}})^\delta \quad (20)$$

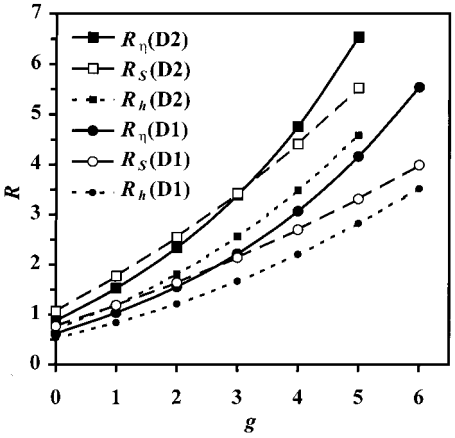

Figure 8. Radius of gyration R_S, the hydrodynamic radius R_h, and the viscometric radius R_η for D1 and D2 dendrimers plotted as a function of the generation g for $\tau B = 0.5$. All values are in bond length units.

and

$$R_{\eta_{max}} = k_{\eta_{max}} (R^{f.d.}_{\eta_{ph}})^\epsilon \quad (21)$$

with different best-fitting parameters for D1 and D2 dendrimers (see Table 3). Inserting eqs 20 and 21 into eq 18, a useful analytical expression for R_η is obtained. Finally, with the parameters reported in Table 1, it is easy to retrieve data for any particular interaction parameter τB and structure (g and P).

Dependence on g and Comparison with Previous Results. For a comparison with experimental and simulation data, we show in Figure 8 the calculated values of the radii for D1 and D2 dendrimers as a function of the generation g. As done before, we report our results for $\tau B = 0.5$, yielding a significant molecular swelling in all dendrimers. Note that a fixed τB, i.e., a fixed strength of the two-body interactions, corresponds to choosing a given monomer/solvent pair at a constant temperature or a fixed interaction potential in computer simulations. The radii of gyration of the phantom molecules change almost linearly with g (see Table 1), whereas in a good solvent they show an upward curvature, in particular for D2 dendrimers. The curvature is basically the same for the hydrodynamic radius, whereas it is more pronounced for the viscometric radius.

Experimental and computer simulation radii of gyration and viscometric radii are reported in Figure 9 as a function of g in comparison with our results for D1 dendrimers at $\tau B = 0.5$. We also show the maximum-expansion radii, $R_{S_{max}}$ and $R_{\eta_{max}}$, and the phantom-molecule radii, $R_{S_{ph}}$ and $R_{\eta_{ph}}$. In both cases, the maximum-expansion values qualitatively follow the same trend as the phantom-molecule results, though being obviously quite larger. Unless otherwise stated, the data by other authors apply to dendrimers having the same topology as ours, namely binary dendra stemming from a ternary core. These data were normalized by suitable segment lengths for a comparison with our results. The fitted lengths are in the expected range, being somewhat shorter than the stretched length of one spacer between consecutive branch points. For instance, in poly(amidoamine), or PAMAM, dendrimers[1] this length amounts[27] to 8.7 Å, to be compared with the value of 6.57 Å we used to normalize both the experimental viscometric radii[27,28] and the radii of gyration obtained by Mansfield

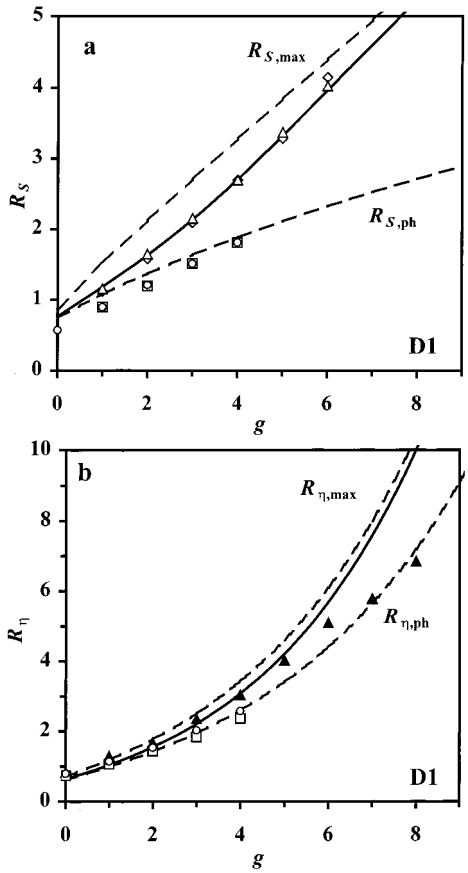

Figure 9. Calculated radius of gyration R_S (a) and viscometric radius R_η (b) in bond length units plotted vs the generation g for D1 dendrimers at $\tau B = 0.5$ (solid lines). The calculated upper and lower limits at maximum expansion and for the phantom molecule are also shown with dashed lines. The symbols report normalized experimental and simulation results for poly(amidoamine), or PAMAM, and poly(propyleneimine), or PPI, dendrimers (see text). Empty triangles: MK Monte Carlo simulations of PAMAM dendrimers[29] normalized by 6.57. Filled triangles: experimental results on PAMAM dendrimers[27,28] normalized by 6.57. Diamonds: MG molecular dynamics simulations of PAMAM dendrimers[30] normalized by 3.81. Squares: experimental results on nitrile-terminated PPI dendrimers[31] normalized by 6.68. Circles: experimental results on amine-terminated PPI dendrimers[31] normalized by 7.67.

and Klushin in Monte Carlo simulations[29] (MK in the following). In the latter simulations, performed on a diamond lattice, six lattice points were taken between consecutive branch points so as to mimic the chemical structure of PAMAM. The good agreement between the simulation results for R_S and ours is gratifying. On the other hand, some disagreement shows up with the experimental R_η at large g (≥ 7), where our results are extrapolated, and not directly calculated. Moreover, the large density of such molecules may imply some inadequacy of the preaveraging approximation used by us.

A very good agreement is also found between our results for R_S and the molecular dynamics simulations for athermal system performed[30] by Murat and Grest (MG in the following). These authors took seven segments between branch points, as MK did, and performed off-lattice simulations assuming a finite monomer size. Their results, originally given in segment length units, were normalized by 3.81. It is worth noting that the two fitted lengths can be satisfactorily reconciled. In fact, MK adopted[29] for the lattice spacing a value of $3^{1/2}$, and if we correct the segment length fitted to their results by this value so as to express them in bond length units, as MG did, we get a value of 3.79!

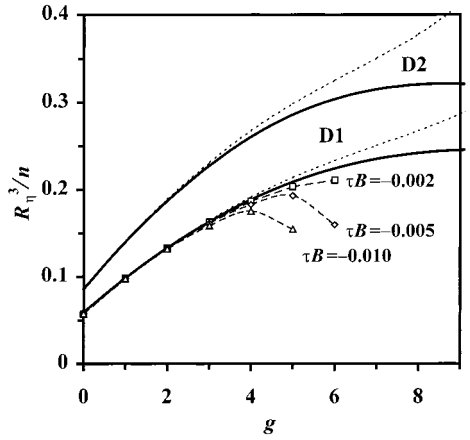

Figure 10. Quantity R_η^3/n, proportional to the intrinsic viscosity (see eq 22), shown as a function of g for the phantom molecule (thick curves) and at a very small expansion ($\tau B = 0.01$, dotted curves). The dashed curves connect the numerical results for D1 dendrimers at slightly negative τB values indicated in the plot.

Figure 9 reports also recent experimental results obtained by Scherrenberg et al.[31] on poly(propylenimine), or PPI, dendrimers either nitrile- or amine-terminated. Note that the segment length values used to scale the experimental data are different for the two dendrimer families: they are 7.67 Å for the amine-terminated and 6.68 Å for the nitrile-terminated dendrimers. The observed radii of gyration and viscometri radii of these samples increase much less with g than hitherto discussed. Indeed, the experimental values for R_η and R_S qualitatively follow the phantom-molecule results. While the different segment lengths can be due to the presence of different terminal groups and/or to the use of different solvents, the closer agreement with the phantom-molecule behavior arises from at least two reasons. The first one is that these samples have a twin core, consisting of a diaminobutane moiety that keeps afar the two halves of the molecule, thus somewhat relieving the steric congestion. Therefore, the molecular topology is not identical with ours. The second reason can be traced down to the short propyl spacers between branch points, much shorter than a statistical segment. Therefore, one expects large stereochemical correlations across the branch points and little excluded-volume effect. In conclusion, our model is not fully adequate for these dendrimers.

The calculated generation dependence of the intrinsic viscosity $[\eta]$ can be analytically expressed through eqs 18−21 and the parameters of Table 3. Figure 10 shows for D1 and D2 dendrimers the calculated curves of the ratio

$$\frac{R_\eta^{\,3}}{n} = [\eta]\frac{3m_{\mathrm{bead}}}{10\pi} \tag{22}$$

with m_{bead} the bead mass. The solid curves apply to phantom molecules and the dotted lines to a small interaction parameter, namely $\tau B = 0.01$ (i.e., a marginally good solvent).

Because of the universal behavior shown through the reduced variable $\beta_\eta \tau B n^{\xi}$, good-solvent expansion produces a larger increase of R_η^3/n (hence of $[\eta]$) the larger is g. Our calculated values do not support any evidence

of a maximum of $[\eta]$ in a good solvent, unlike what is experimentally found in some cases.[28,32] By extrapolation of eq 20, we find that only the values for the phantom molecule display a slow transition to an asymptotic value or possibly a shallow maximum at large g, while good-solvent results do show a steady increase, even at a very small τB (see Figure 10). Thus, slightly negative τB values could produce a maximum of $[\eta]$. Our model is not suited to study the poor-solvent collapse at $\tau B < 0$, because it does not account for many-body repulsive interactions. However, if τB is still very close to 0, these interactions are negligible, and intramolecular contraction is mostly resisted by configurational entropy. Therefore, we performed exploratory calculations on D1 dendrimers for τB in the range -0.002 to -0.01. A maximum for R_η^3/n does indeed appear at $g = 4$ for $\tau B = -0.01$ or at $g = 5$ for $\tau B = -0.005$. The relevant conclusion is that poor solvent conditions or the effect of the terminal groups (chemically different from the dendrimer backbone) may produce a maximum of $[\eta]$ at a low generation.[28,32] We also point out that even minute amounts of statistical defects in the chemical synthesis produce relatively large quantities of lower mass impurities at high generations.[2] These defective structures may significantly[7] decrease $[\eta]$ at large g, thus possibly producing the observed maximum.

Concluding Remarks

In this paper we theoretically study the good-solvent expansion of dendrimers with the topology reported in Scheme 1 using self-consistent free energy minimization. Accounting for all the relevant degrees of freedom, we investigate the overall behavior of these sterically congested molecules in terms both of their overall size and of the local conformation. We find that the intramolecular expansion is mostly concentrated in the core region, all dendra (or sub-dendra, etc.) being somewhat stretched outward, with relatively little mixing.

The calculated radii of gyration and viscometric radii fall on single master curves when the reduced variables $\beta_S \tau B n^\varphi$ or $\beta_\eta \tau B n^\xi$ are used (see Tables 2, 3 and Figures 5, 7). Here, the β prefactors are related to the number of bonds between branch points (one or two in our case), while the exponents are comprised between the value of 0.5, appropriate for linear and star polymers, and of 1, valid for two-dimensional polymers. The master curves can be analytically described through universal Hill functions, enabling a simple computation of the radii for any chosen generation, topology, and solvent quality. It should be stressed that our universal equations describe very accurately the results of two different families of dendrimers, both from very low to congested generation and from null to asymptotic (maximum) expansion. Such features are not found in other treatments of experimental or simulations data, which are described analytically through simple scaling laws.

Within our coarse-grained model, the beads interact through two-body interactions only. These repulsive contributions induce molecular swelling, with a simultaneous loss of configurational entropy. The equilibrium state is achieved through balance of these opposite requirements. Because of the sterically congested nature of the dendrimers, the problem arises of the importance of many-body, or at least of three-body, interactions. In keeping with the usual practice for linear and star polymers, we did not include explicitly these interactions to study the good-solvent behavior. The rationale is that a large share of three-body interactions involves two topologically close chain atoms because of molecular connectivity. These interactions are already embodied by the two-body interactions *between the beads*, each bead comprising a few neighboring atoms.

On the other hand, three-body interactions are essential to investigate the Θ state, defined by the vanishing of the second virial coefficient. In this case, the Θ temperature may be calculated by requiring that the *inter*molecular two- and three-body interactions do compensate one another. Because of residual *intra*molecular three-body interactions, and in analogy to what is found in star polymers,[33] we expect the phantom molecule to be a rather poor approximation of the real conformation at the Θ temperature. Investigation of dendrimer behavior in such conditions remains an open theoretical and experimental issue.

Acknowledgment. F.G. gratefully acknowledges the financial support by CNR (Consiglio Nazionale delle Ricerche, Italy) Project "Materiali Speciali per Tecnologie Avanzate II".

Appendix

Structural Symmetries and Bond Parental Relationships. Within our statistical approach, we may consider only the topologically nonequivalent bonds (or beads) pairs. Exploiting the parental relationships, topological equivalences can be easily established for symmetrical and regular graph structures whose terminal vertexes extend to the same shell, i.e., to the same topological distance from the core. The parental relationship between any two beads i, j can be established by a triad of values: the shells s_i and s_j the beads belong to and the shell s_a of their common ancestor. For beads belonging to the same generation sequence (i.e., one sprouting from the other), the common ancestor is simply $s_a = \min(s_i, s_j)$. Therefore, the total number of topologically different bead pairs does not depend on the core or on the branch multiplicity. The number of nonequivalent bead pairs is

$$C_{\text{beads}} = (g+1)(g+2)(g+6)P^2/6 - (g+1)(g+4)P(P-1)/4 \quad \text{(A-1)}$$

and the number of nonequivalent bond pairs to be optimized is

$$C_{\text{bonds}} = (g+1)(g^2+8g+6)P^2/6 - g(g+1)P(P-1)/4 \quad \text{(A-2)}$$

which readily becomes a small fraction of all the possible pairs, $(n-1)(n-2)/2$. Depending on the bond numbering pattern,[7] suitable algebraic expressions are obtained for mapping any couple of bond indices into the reduced array of independent bond pairs, and vice versa.

In this way, we achieve the most efficient simplification of the numerical procedure in terms of the chosen variables. On the other hand, in nonsymmetrical structures, all bead or bond pairs must be considered, with a large number of variables to be handled in multidimensional optimization procedures.

Numerical Free Energy Optimization. Even when the average structural symmetry of dendrimers is fully exploited through the parental relationships, the number of variables to be optimized is quite large in high-

generation dendrimers. Therefore, the free energy minimization is carried out through a simple iterative algorithm which independently optimizes one scalar product after the other at each cycle. No simultaneous optimization of the variables was found necessary, as checked through use of a local version of the powell routine of ref 34 by considering the full set of variables. Note in fact that a number of actual distances and scalar products do already change collectively with each optimized variable due to the parental relationships. In all cases, convergence was achieved when the relative free energy difference from iteration i to iteration $(i + 1)$ satisfied the inequality

$$2\frac{|A_{(i+1)} - A_{(i)}|}{|A_{(i+1)} + A_{(i)}|} \leq \epsilon$$

with ϵ equal to 10^{-7}.

References and Notes

(1) Tomalia, D. A.; Naylor, A. M.; Goddard, W. A., III *Angew. Chem., Int. Ed. Engl.* **1990**, *29*, 138.
(2) Bosman, A. W.; Janssen, H. M.; Meijer, E. W. *Chem. Rev.* **1999**, *99*, 1665.
(3) de Gennes, P. G.; Hervet, H. *J. Phys., Lett.* **1983**, *44*, L351.
(4) Ganazzoli, F. *J. Chem. Phys.* **1998**, *108*, 9924.
(5) Allegra, G.; Ganazzoli, F. *Adv. Chem. Phys.* **1989**, *75*, 265.
(6) Ganazzoli, F.; La Ferla, R.; Raffaini, G., manuscript in preparation.
(7) La Ferla, R. *J. Chem. Phys.* **1997**, *106*, 688.
(8) Raos, G.; Allegra, G.; Ganazzoli, F. *J. Chem. Phys.* **1994**, *100*, 7804.
(9) Allegra, G.; Colombo, E.; Ganazzoli, F. *Macromolecules* **1993**, *26*, 330.
(10) Zimm, B. H. *J. Chem. Phys.* **1956**, *24*, 269.
(11) Doi, M.; Edwards, S. F. *The Theory of Polymer Dynamics*; Oxford Scientific Publications: Oxford, 1986.
(12) Yamakawa, H. *Modern Theory of Polymer Solutions*; Harper & Row: New York, 1971.
(13) Forni, A.; Ganazzoli, F.; Vacatello, M. *Macromolecules* **1996**, *29*, 2994.
(14) Forni, A.; Ganazzoli, F.; Vacatello, M. *Macromolecules* **1997**, *30*, 4737.
(15) Zifferer, G. *Macromol. Theory Simul.* **1994**, *3*, 163; **1999**, *8*, 433.
(16) Mansfield, M. L. *Polymer* **1994**, *35*, 1827.
(17) Zimm, B. H. *Macromolecules* **1980**, *13*, 592; **1984**, *17*, 795.
(18) Freire, J. J.; Rey, A.; Bishop, M.; Clarke, J. H. R. *Macromolecules* **1991**, *24*, 6494.
(19) Ganazzoli, F.; Allegra, G.; Colombo, E.; De Vitis, M. *Macromolecules* **1995**, *28*, 1076.
(20) Shimada, J.; Yamakawa, H. *J. Polym. Sci., Polym. Phys. Ed.* **1978**, *16*, 1927.
(21) The Nobel Prize winner Archibald V. Hill (1886−1977) used the equation that bears his name in the study of binding equilibria. See: Hill, A. V. *J. Physiol. (London)* **1910**, *40*, iv−vii. The same equation is used for the description of pharmacological dose−effect relationships in the presence of saturation effects.
(22) Chen, Z. Y.; Cui, S.-M. *Macromolecules* **1996**, *29*, 7943.
(23) Boris, D.; Rubinstein, M. *Macromolecules* **1996**, *29*, 7251.
(24) de Gennes, P. G. *Scaling Concepts in Polymer Physics*; Cornell University Press: Ithaca, NY, 1979.
(25) des Cloizeaux, J.; Jannink, G. *Les Polymères en Solution: leur Modélisation et leur Structure*; Les Editions de Physique: Paris, 1987.
(26) Lescanec, R. L.; Muthukumar, M. *Macromolecules* **1990**, *23*, 2280.
(27) Mansfield, M. L.; Klushin, L. I. *J. Phys. Chem.* **1992**, *96*, 3994.
(28) Tomalia, D. A.; Hedstrand, D. M.; Wilson, L. R. *Encyclopedia of Polymer Science and Engineering*, 2nd ed.; Wiley: New York, 1990; Index Vol., pp 46−92.
(29) Mansfield, M. L.; Klushin, L. I. *Macromolecules* **1993**, *26*, 4262.
(30) Murat, M.; Grest, G. S. *Macromolecules* **1996**, *29*, 1278.
(31) Scherrenberg, R.; Coussens, B.; van Vliet, P.; Edouard, G.; Brackman, J.; de Brabander, E.; Mortensen, K. *Macromolecules* **1998**, *31*, 456.
(32) Mourey, T. H.; Turner, S. R.; Rubinstein, M.; Fréchet, J. M. J.; Hawker, C. J.; Wooley, K. L. *Macromolecules* **1992**, *25*, 2401.
(33) Ganazzoli, F. *Macromolecules* **1992**, *25*, 7357.
(34) Press, W. H.; Teukolsky, S. A.; Vetterling, W. T.; Flannery, B. P. *Numerical Recipes in Fortran*; Cambridge University Press: Cambridge, UK, 1992.

MA000258+